Journal of Translational Medicine

RESEARCH

Open Access

N-acetyltransferase 10 affects the proliferation of intrahepatic cholangiocarcinoma and M2-type polarization of macrophages by regulating C-C motif chemokine ligand 2

Teng Cai[1,2], Jianye Dai[3], Yanyan Lin[4], Zhongtian Bai[4,5*], Jingdong Li[2*] and Wenbo Meng[4,5*]

Abstract

Background N-acetyltransferase 10 (NAT10) plays a crucial role in the occurrence and development of various tumors. However, the current regulatory mechanism of NAT10 in tumors is limited to its presence in tumor cells. Here, we aimed to reveal the role of NAT10 in intrahepatic cholangiocarcinoma (ICC) and investigate its effect on macrophage polarization in the tumor microenvironment (TME).

Methods The correlation between NAT10 and ICC clinicopathology was analyzed using tissue microarray (TMA), while the effect of NAT10 on ICC proliferation was verified in vitro and in vivo. Additionally, the downstream target of NAT10, C-C motif chemokine ligand 2 (CCL2), was identified by Oxford Nanopore Technologies full-length transcriptome sequencing, RNA immunoprecipitation-quantitative polymerase chain reaction, and coimmunoprecipitation experiments. It was confirmed by co-culture that ICC cells could polarize macrophages towards M2 type through the influence of NAT10 on CCL2 protein expression level. Through RNA-sequencing, molecular docking, and surface plasmon resonance (SPR) assays, it was confirmed that berberine (BBR) can specifically bind CCL2 to inhibit ICC development.

Results High expression level of NAT10 was associated with poor clinicopathological manifestations of ICC. In vitro, the knockdown of NAT10 inhibited the proliferative activity of ICC cells and tumor growth in vivo, while its overexpression promoted ICC proliferation. Mechanically, by binding to CCL2 messenger RNA, NAT10 increased CCL2 protein expression level in ICC and their extracellular matrix, thereby promoting the proliferation of ICC cells and M2-type polarization of macrophages. BBR can target CCL2, inhibit ICC proliferation, and reduce M2-type polarization of macrophages.

*Correspondence:
Zhongtian Bai
ldyy_baizht@lzu.edu.cn
Jingdong Li
lijingdong358@126.com
Wenbo Meng
mengwb@lzu.edu.cn

Full list of author information is available at the end of the article

Conclusions NAT10 promotes ICC proliferation and M2-type polarization of macrophages by up-regulating CCL2, whereas BBR inhibits ICC proliferation and M2-type polarization of macrophages by inhibiting CCL2.

Keywords NAT10, Intrahepatic cholangiocarcinoma, CCL2, Berberine, Macrophage

Introduction

Cholangiocarcinoma (CCA) is a highly aggressive malignancy that originates from the bile duct epithelium. It accounts for approximately 3% of all gastrointestinal malignancies and can be categorized based on its anatomic location of origin into intrahepatic CCA (ICC), perihilar CCA, and distal CCA [1, 2]. ICC accounts for 10% of all primary liver cancers [1], and its incidence is increasing [3, 4]. Surgical resection is the only possible curative treatment, and the 5-year overall survival rate is reportedly 15–40% [5]. However, up to two-thirds of patients will relapse after surgical removal [6]. Although gemcitabine combined with cisplatin is effective in patients who do not undergo surgery or require adjuvant chemotherapy, the median survival in these patients is only 11.8 months [7]. Additionally, no targeted therapy for ICC exists. Therefore, uncovering the pathogenesis and identifying therapeutic targets is a burning question for the treatment of ICC.

Recently, the role of RNA acetylation, particularly N4-acetylcytidine (ac4C) modification, in tumors has begun to attract attention. N-acetyltransferase 10 (NAT10), a GCN55-related N-acetyltransferase, is the only writer of ac4C. It has an acetyltransferase domain and a lysine-rich carboxyl terminus. NAT10 plays a critical role in mRNA stability and translation efficiency by modifying mRNA with ac4C [8]. Multiple studies have examined how NAT10 regulates tumor progression by modifying mRNA with ac4C [9–12]. However, its regulating pattern in ICC and the tumor microenvironment (TME) remains unclear. The TME is composed of all noncancerous host cells and non-cellular components in the tumor and plays an important role in the occurrence and development of tumors. Additionally, macrophages are an important component of the TME. They are mainly categorized into two states with opposite functions as follows: M1 (pro-inflammatory, usually antitumor) and M2 (anti-inflammatory, pro-tumor) macrophages [13]; they can be transformed into each other [14].

Tumor-associated macrophages (TAMs) are macrophages that invade cancerous tissues and aid in cancer progression, usually exhibiting an M2 phenotype [15]. The infiltration of macrophages into tumor tissue is primarily driven by the recruitment of the C-C motif chemokine ligand 2 (CCL2) in the TME, which binds to the C-C motif chemokine receptor 2 (CCR2) on the surface of the cells, polarizing them into M2 macrophages. M2 macrophages induced by CCL2 also secrete CCL2, thereby promoting the infiltration of more macrophages into the tumor and their polarization toward the M2 phenotype [16, 17]. In addition to secreting CCL2, M2 macrophages also release cytokines, such as vascular endothelial growth factor (VEGF), platelet-derived growth factor (PDGF), and transforming growth factor-β (TGF-β), which promote tumor cell epithelial-mesenchymal transition (EMT), angiogenesis, and extracellular matrix (ECM) remodeling [18, 19], thereby influencing the TME.

CCL2, also known as monocyte chemoattractant protein-1 (MCP-1), belongs to the CC chemokine family and can recruit monocytes, dendritic cells, and memory T cells to inflammation sites [20, 21]. Studies have indicated that CCL2 plays a role in promoting pathological angiogenesis, tumor cell survival and invasion, and immunosuppressive cell recruitment [22–24]. In various tumors, CCL2 expression is elevated and can induce macrophage polarization toward the M2 phenotype through extracellular secretion [25–27]. However, CCL2 expression and whether ICC cells can influence macrophage polarization via CCL2 has not been reported in CCA, particularly ICC. Since our previous experiments, including RNA sequencing, identified CCL2 as a downstream target of NAT10 in ICC cells, we conducted related studies to investigate whether ICC cells can regulate CCL2 expression through NAT10 to affect macrophage polarization. The intracellular distribution of NAT10 is mainly located in the nucleolar region, which affects the progression of tumor cells by regulating other proteins or pathways. Therefore, this study aimed to uncover the specific regulatory mechanisms of NAT10 in ICC and its relationship with TME.

Materials and methods

Cholangiocarcinoma (CCA) specimens and cell lines

The human ICC cell lines RBE and HuCCT1 were purchased from Shanghai Fu Heng Biological (Shanghai, China) and cultured in RPMI-1640 medium (Hyclone, USA) with 10% fetal bovine serum (FBS) (Biosharp, China) and 1% penicillin-streptomycin (Biosharp, China) at 5% CO_2 and 37 °C. Macrophage RAW264.7 cells were purchased from Wuhan Procell Life Science & Technology Co., Ltd. (Wuhan, China) and cultured in a special medium (CM-0190, Procell). All cell lines were authenticated through short tandem repeats (STR) profiling. The CCA tissue microarray (TMA) containing 90 CCA and 31 interlobular bile duct tissues with complete clinicopathological information was purchased from Shanghai Outdo Biotech Co., Ltd. (Shanghai, China).

Construction of stable knockdown and overexpressing cell lines

NAT10 overexpression and knockdown lentiviruses were purchased from Genechem Co., Ltd. (Shanghai, China), and CCL2 overexpression and knockdown lentiviruses were purchased from Genecarer Biotech Co., Ltd. (Xi 'an, China). Transfection was performed according to the manufacturer's instructions. Stable clones were screened with 2 μg/mL of puromycin (HY-B1743A, MCE) for at least 1 week. Knockdown and overexpression were validated at the RNA and protein levels. Supporting Table 1 presents the short hairpin RNAs used in this study.

Quantitative real-time polymerase chain reaction

Total RNA was extracted using Trizol reagent (15596026CN, Invitrogen). cDNA synthesis was performed using PrimeScript RT Master Mix (RR036A, Takara). The obtained cDNA was used as a template for quantitative reverse transcription polymerase chain reaction (qRT-PCR) using TB Green Premix Ex Taq II (RR820A; Takara). The relative RNA expression was normalized to GAPDH using the $2^{-\Delta\Delta Ct}$ method. Primers used in this study are listed in Supporting Table 1.

Table 1 Correlation between NAT10 expression and clinicopathological features of CCA

Variables	No. of patients (%)	NAT10 expression		*p*
		Low *n* = 57(%)	High *n* = 33(%)	
Age				
< 65	72(80.0)	47(82.5)	25(75.8)	0.444
≥ 65	18(20.0)	10(17.5)	8(24.2)	
Gender				
Male	47(52.2)	27(47.4)	20(60.6)	0.226
Female	43(47.8)	30(52.6)	13(39.4)	
Tumor location				
ICC	25(27.8)	20(35.1)	5(15.2)	0.032*
pCCA	58(64.4)	35(61.4)	23(69.7)	
dCCA	7(7.8)	2(3.5)	5(15.2)	
Differentiation				
Poor	5(5.6)	3(5.3)	2(6.1)	0.042*
Moderate	67(74.4)	38(66.7)	29(87.9)	
Well	18(20.0)	16(28.1)	2(6.1)	
Vascular invasion				
Absent	61(67.8)	37(64.9)	24(72.7)	0.445
Present	29(32.2)	20(35.1)	9(27.3)	
Primary tumor (T)				
T1	7(7.8)	6(10.5)	1(3.0)	0.035*
T2	62(68.9)	42(73.7)	20(60.0)	
T3	18(20.0)	9(15.8)	9(27.3)	
T4	3(3.3)	0(0.0)	3(9.1)	
Recurrence				
Lost	3(3.3)	2(3.5)	1(3.0)	0.987
Yes	55(61.1)	35(61.4)	20(60.6)	
No	32(35.6)	20(35.1)	12(36.4)	

Western blotting

Cells were lysed in RIPA lysis buffer (#9806, Cell Signaling Technology) and centrifuged at 12 000 × g at 4 °C for 30 min. The supernatant was collected, and the protein concentration was determined using a bicinchoninic acid protein assay (abs9232, Absin). Total protein samples (50 μg) were subjected to Tris-glycine sodium dodecyl sulfate–polyacrylamide gel electrophoresis (10% and 12% for NAT10 and CCL2, respectively) (CW0022M, CWBIO) and then transferred onto PVDF membranes (AR1152-10, Boster). After blocking with 5% non-fat milk, the membranes were incubated overnight at 4 °C with primary antibodies anti-NAT10 (1:2000, ab194297, Abcam) and anti-CCL2 (1:1000, ab214819, Abcam). After three washes with Tris-buffered saline with 0.1% Tween® 20 detergent (AR0195-10, Boster), the membranes were incubated with a secondary antibody for 1 h, and bands were visualized using enhanced chemiluminescence detection reagent (AR1197, Boster). Protein band intensity was quantified using ImageJ software (Bethesda, Maryland, USA), and relative protein expression was normalized to GAPDH.

Cell proliferation, live-cell imaging, and colony formation assays

For the cell proliferation assays, 2×10^3 cells were inoculated into 96-well plates and cell proliferation was measured for 5 consecutive days to evaluate cell proliferation activity using a Cell Counting Kit-8 (CCK-8) (K1018, APExBIO). For live-cell imaging, 1×10^3 cells were inoculated into a 96-well plate using a Cytation 1 imaging system (BioTek, USA). Images were taken every 2 h for 5 days. Finally, the total number of cells was counted to evaluate cell proliferation. Cells were seeded in 6-well plates for colony formation assays. The numbers of knockdown and overexpression cells were 800 and 500, respectively. After 8–12 days, the cells were fixed with 4% paraformaldehyde (DF0135, LEAGENE), subjected to crystal violet staining (G1063, Solarbio), and photographed. Finally, the colonies were counted.

Animal studies

All animal experiments were approved by the Ethics Committee of the First Hospital of Lanzhou University (approval number: LDYYLL-2024-38) and complied with the Code of Ethics for Animal Experiments. All nude mice were purchased from Jiangsu GemPharmatech Co.,Ltd. (Nanjing, China). In vivo experiments were conducted in male BALB/c nude mice aged 4–5 weeks to analyze the effects of NAT10 and CCL2 on ICC. HuCCT1-shNC, HuCCT1-shNAT10#1, and HuCCT1-shCCL2 cells (1×10^7/100 μL per mouse, $n=6$ per group) suspended in pre-cooled serum-free RPMI-1640 medium (Hyclone, USA) were injected subcutaneously into the

flanks of mice. Changes in subcutaneous tumor volume ($V=0.5 \times L \times W^2$) were closely monitored. At the end of the experiment, the mice were sacrificed through the injection of excess pentobarbital sodium, and the tumors were removed and weighed. The tumors were resected for hematoxylin and eosin (H&E) staining, immunohistochemistry (IHC), immunofluorescence, and Western blot.

H&E staining, IHC, and immunofluorescence

Tissue samples were fixed with 4% paraformaldehyde (DF0135, LEAGENE), embedded in paraffin, and sectioned for H&E staining, IHC, and immunofluorescence. During IHC, the TMA and xenograft tumor tissues were successively dewaxed, hydrated, subjected to antigenic repair and serum blocking, and incubated at 4 °C with primary antibody overnight. The primary antibodies used were anti-NAT10 (1:500, ab194297, Abcam) and anti-CCL2 (1:200, 25542-1-AP, Proteintech). Subsequently, the slices were incubated with the secondary antibody for 30 min and further incubated with 3,3′-diaminobenzidine and hematoxylin. Finally, tissue sections were photographed and analyzed. The expression intensity of NAT10 was determined independently by two senior pathologists who were blinded to the clinicopathological data. Specifically, the expression of NAT10 was quantified using the H-score as follows: H-score = π(i+1), where π is the percentage of positive cells and i is the staining intensity (0–3). The staining intensity was classified into the following four grades: 0, negative expression; 1, weak expression; 2, moderate expression; and 3, strong expression. Finally, the samples were classified as having low or high expression based on the median H-score.

For immunofluorescence, xenograft tumor sections underwent dewaxing, hydration, antigen repair, and incubation in 3% H_2O_2 at 37 °C for 25 min to inhibit endogenous peroxidase. Next, the sections were incubated with 3% bovine serum albumin at room temperature for 30 min, and the primary and corresponding secondary antibodies were administered successively. The following antibodies were used: F4/80 (1:200, 28463-1-AP, Proteintech), CD86 (1:200, 13395-1-AP, Proteintech), and CD163 (1:200, ab182422, Abcam).

Oxford Nanopore Technologies full-length transcriptome sequencing

Oxford Nanopore Technologies (ONT) full-length transcriptome sequencing was performed on NAT10-knockdown (shNAT10#1 and shNAT10#2) and control (shNC) RBE cells. The experiments were performed according to the standard protocol provided by Oxford Nanopore Technologies, including sample quality inspection, library construction, library quality inspection, and library sequencing. Specifically, the DESeq R software package (1.10.1) was used to analyze the differential expression between the two conditions. A fold change ≥ 1.5 and $P<0.05$ was defined as significantly differentially expressed. Gene Ontology (GO) and Kyoto Encyclopedia of Genes and Genomes (KEGG) signaling pathway enrichment analyses were performed on the differentially expressed genes. GO enrichment analysis was performed using the GOseq R packet based on the Wallenius non-central hypergeometric distribution [28]. KEGG pathway enrichment analysis of differentially expressed genes was performed using KOBAS software [29]. ONT full-length transcriptome sequencing was accomplished by Beijing BMKCloud (www.biocloud.net).

RNA immunoprecipitation-quantitative polymerase chain reaction

HuCCT1 cells and the Imprint® RNA Immunoprecipitation Kit (SAB4200085, Merck Millipore) were used for this assay. HuCCT1 cells were transfected according to the manufacturer's instructions, and samples were collected 48 h later. The sample and 5 μg of anti-NAT10 antibody (ab194297, Abcam) were added to magnetic beads, and the samples were incubated at room temperature for 30 min. Next, the beads were washed two times with washing buffer, and then RNA immunoprecipitation (RIP) buffer was added. The immune complex was obtained by adding the cell lysate to the magnetic bead-antibody complex. Finally, the immune complex was separated using washing buffer and the RNA was used for quantitative polymerase chain reaction.

Coimmunoprecipitation assay

HuCCT1 cells were lysed on ice with immunoprecipitation lysis buffer for 30 min and then centrifuged at 4 °C at 14 000 rpm for 30 min to collect the supernatant. Anti-NAT10 (ab194297, Abcam) or control IgG was added, and the samples were incubated at 4 °C overnight. Subsequently, 30 μL of beads were added, and the sample was rotated overnight at 4 °C. The beads were washed three times with cracking buffer, and the supernatant was collected for western blotting.

Enzyme-linked immunosorbent assay

The levels of CCL2 in the cell supernatants were determined using an enzyme-linked immunosorbent assay (ELISA) kit (E-EL-H6005, Elabscience). First, a reference standard working solution was used to construct a standard curve. The cell supernatant was then analyzed according to the manufacturer's instructions. After adding the substrate solution, the plate was incubated at 37 °C for approximately 15 min, depending on the color development. Finally, the Stop Solution was added, and the optical density was measured at 450 nm using a microplate reader (synergy H1, BioTek, USA).

Molecular docking

The structure of berberine (BBR) was downloaded from PubChem, and the three-dimensional (3D) structures of NAT10 (Protein Data Bank [PDB]: 0000) and CCL2 (PDB: 1DOL) were obtained from the RCSB PDB. Next, the protonation state of the small molecule was set at pH 7.4, and the compound was extended to a 3D structure using Open Babel [30]. The AutoDock tool (ADT3) was used to prepare the receptor proteins and ligands. Additionally, the docking box was generated using the AutoGrid program, and molecular docking was performed using AutoDock Vina (1.2.0) [31]. The optimal combination conformation was selected to analyze the interactions. Finally, a protein-ligand interaction diagram was generated using the PyMOL software [32].

RNA sequencing after BBR treatment

HuCCT1 cells were treated with 20 μM of BBR for 48 h, and RNA was harvested. RNA sequencing was performed by Wuhan Ruixing Biotechnology Co., Ltd. (Wuhan, China). Illumina Novaseq 6000 was used for high-throughput sequencing in PE150 mode. The DESeq2 software package was used to analyze the differential expression between the two groups [33]. Fold change≥2 or ≤1/2 and $P<0.05$ were used as the screening criteria. Differentially expressed genes were analyzed using GO (http://geneontology.org/) and KEGG (http://www.kegg.jp/).

Surface plasmon resonance

Surface plasmon resonance (SPR) was performed using a Biacore T20 (GE Healthcare) and a CM5 chip. After replacing the new CM5 chip, it was cleaned with NaOH, activated, protein-coupled, and sealed. Finally, the buffer and sample were run, and an affinity test was performed. The low-molecular-weight kinetics model was selected for sample injection. SPR was accomplished by Shanghai OLBIOTECH (Shanghai, China).

Toxicity testing

BBR (HY-17577, MCE) was diluted to various concentrations (0, 10, 20, 40, 80, 160, and 200 μM) and used to treat the ICC cells for different durations (24, 48, 72, and 96 h). The inhibitory effect of BBR on ICC cells was assessed using the CCK-8 assay (K1018, APExBIO). Next, the concentration of the drug that inhibits 50% of the effect was determined as IC50 and analyzed using GraphPad Prism 8.0 software (San Diego, CA, USA). We used live-cell imaging to assess the inhibitory effects of BBR on the proliferation of RBE (80 and 160 μM) and HuCCT1 (10 and 20 μM) cells.

Flow cytometry

RBE (80 and 160 μM) and HuCCT1 (10 and 20 μM) cells were treated with BBR for 48 h. Cell cycle (C1052, Beyotime) and apoptosis (E-CK-A211, Elabscience) kits were used to collect and stain the cells according to the manufacturer's instructions. Flow cytometry was performed using an Agilent flow cytometer (Palo Alto, CA, USA). To detect macrophage polarization, macrophages were co-cultured with ICC cells in a transwell chamber. After 24 h, macrophages were collected and incubated with CD86 (0.125 μg/test, 12-0862-82, Invitrogen) and CD206 (0.25 μg/test, 17-2061-80, Invitrogen) antibodies at 4 °C for 30 min. Macrophage polarization was analyzed using an Agilent flow cytometer (Palo Alto, CA, USA).

Antitumor effect of BBRin vivo.

HuCCT1 cells (1×10^7) were suspended in 100 μL of serum-free RPMI-1640 medium (Hyclone, USA) and injected subcutaneously into the right forelimb of male BALB/c nude mice aged 4–5 weeks. The tumor size was closely monitored, and when it reached approximately 5 mm^3, the mice were randomly divided into two groups ($n=6$). BBR was administered orally (50 mg/kg/day), and sterile water containing dimethyl sulfoxide (DMSO) (D8371, Solarbio) was administered to the control group. Tumor volume and animal weight were measured every 3 days. Mice were sacrificed approximately 18 days after treatment, and the tumors were removed and weighed. The resected tumors were used for subsequent experiments.

Statistical analysis

All statistical analyses were performed using GraphPad Prism 8.0 (San Diego, CA, USA) and IBM SPSS Statistics for Windows, version 20.0 (IBM Corp., Armonk, N.Y., USA). Differential gene expression and survival analyses were performed using the GEPIA2 tool [34] (http://gepia2.cancer-pku.cn). All data were expressed as mean±standard deviation (SD) and were analyzed using Student's t-test or one-way analysis of variance (ANOVA). The relationship between NAT10 expression and clinicopathological parameters was determined using the chi-square test. Statistical significance was set at $P<0.05$.

Results

NAT10 is upregulated in CCA

Surfing in The Cancer Genome Atlas (TCGA) database, we found that NAT10 was significantly upregulated in CCA ($P<0.05$) (Fig. 1A) and various other solid tumors of the digestive system in TCGA, including stomach adenocarcinoma (STAD), colon adenocarcinoma (COAD), and rectum adenocarcinoma (READ) (Fig. 1B). No difference in overall survival (OS) or disease-free survival (DFS) was found between patients with CCA with high

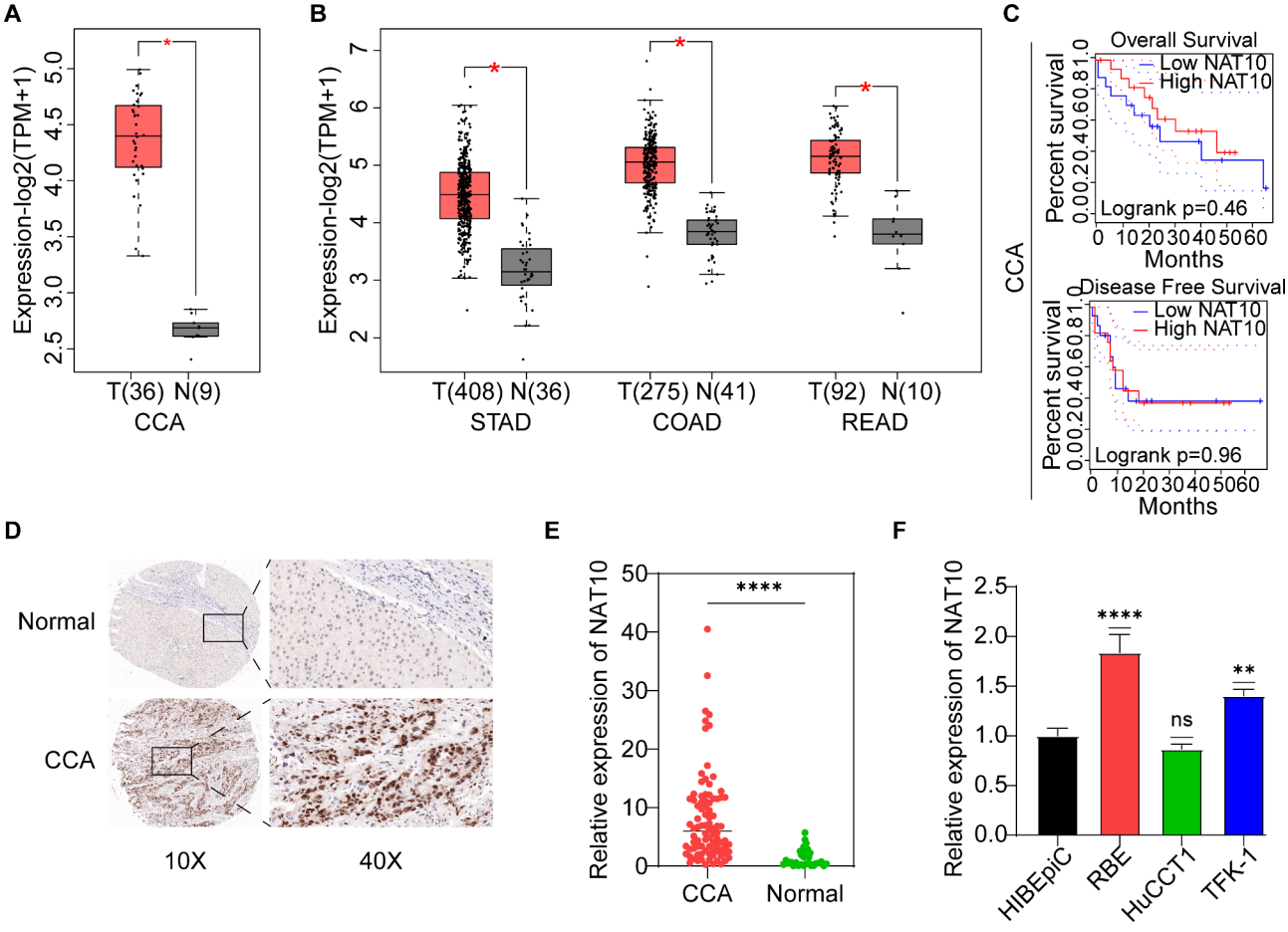

Fig. 1 NAT10 is significantly upregulated in human CCA. (A) NAT10 is upregulated in CCA as compared to adjacent normal tissue (TCGA data). (B) NAT10 is upregulated in STAD, COAD, and READ as compared to adjacent normal tissue (TCGA data). (C) No significant correlation was found between NAT10 expression and OS or DFS in patients with CCA. (D) Representative images of NAT10 immunohistochemistry (IHC) staining on tissue microarray (TMA). Scale bars: 100 (left panel) and 20 (right panel) μm. (E) NAT10 IHC staining scores of the CCA and matched normal tissues; the expression of NAT10 was indicated by the proportion of positive area. (F) Expression of NAT10 in different CCA cell lines and normal bile duct cells. Data are representative of three or more independent experimental replicates. Data are displayed as the mean ± SD. *P*-values were determined by Student's t-test and one-way ANOVA in panels. $^{*}P < 0.05$, $^{**}P < 0.01$, $^{****}P < 0.0001$, ns: Not significant; TCGA, The Cancer Genome Atlas; CCA, cholangiocarcinoma; OS, overall survival; DFS, disease-free survival; STAD, stomach adenocarcinoma; COAD, colon adenocarcinoma; READ, rectum adenocarcinoma; SD, standard deviation; ANOVA, analysis of variance

and low NAT10 expression. However, patients with high NAT10 expression had significantly poorer OS and DFS than those with low NAT10 expression in most solid tumors, including adrenocortical carcinoma (ACC), head and neck squamous cell carcinoma (HNSC), kidney chromophobe (KICH), kidney renal papillary cell carcinoma (KIRP), liver hepatocellular carcinoma (LIHC), and uveal melanoma (UVM) (Fig. 1C, Supplementary Fig. 1). The reasons for this result could be attributed to the high degree of malignancy of CCA, late stage at which the patient is diagnosed with no chance of surgery, short survival time, and small number of samples in the database.

The TMA of 90 patients with CCA and corresponding adjacent tissues was used to further verify the expression of NAT10 and its clinicopathological features. Notably, the data showed increased NAT10 expression in CCA tissues (Fig. 1D, E), and NAT10 expression was significantly correlated with tumor location, histological grade, and primary tumor stage (Table 1). Quantitative real-time polymerase chain reaction (qRT-PCR) data showed that NAT10 was upregulated in CCA cells (RBE and TFK-1) compared to bile duct epithelial cells (HIBEpiC) (Fig. 1F).

NAT10 promotes the growth of ICC in vivo and in vitro

To investigate the functional role of NAT10 in ICC, we constructed three independent short hairpin RNA (shRNA) sequences (shNAT10#1, shNAT10#2, and shNAT10#3). ShNAT10#1 and shNAT10#2 were selected for subsequent experiments owing to their silencing efficiency (Fig. 2A, B). Additionally, we constructed NAT10-overexpressing cell lines and validated them at

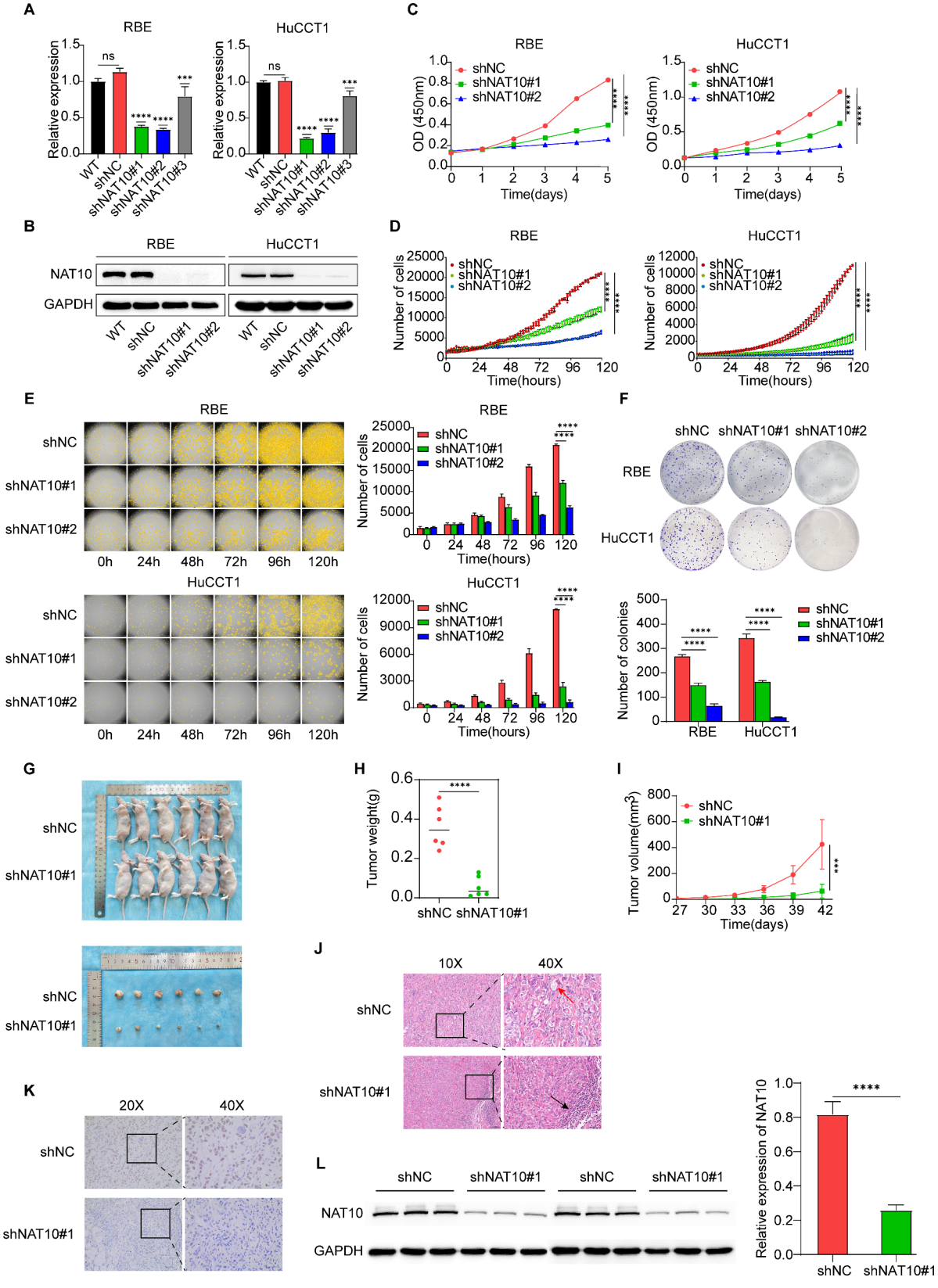

Fig. 2 (See legend on next page.)

(See figure on previous page.)

Fig. 2 Knocking down NAT10 inhibits ICC cell proliferation and tumor growth in mice. (A and B) NAT10-knockdown cell lines were constructed and verified at the mRNA and protein levels by qRT-PCR and western blot, respectively. (C) CCK-8 assays showed that knocking down NAT10 significantly inhibited the proliferation of ICC cells. (D and E) Live-cell imaging showed that knocking down NAT10 significantly inhibited the proliferation of ICC cells. Scale bars: 1000 μm. (F) Knocking down NAT10 significantly reduced the colony-formation ability of ICC cells. (G-I) Knocking down NAT10 effectively inhibited the growth of ICC subcutaneous tumors. Tumor size was measured every 3 days ($n=6$). (J) H&E staining of the subcutaneous tumor tissues in nude mice after NAT10 knockdown. The red and black arrows show angiogenesis and tumor cell necrosis, respectively. Scale bars: 100 (left panel) and 50 (right panel) μm. (K and L) IHC and western blot showing the expression of NAT10 in mouse tumor tissues. Scale bars: 40 μm. Data are representative of three or more independent experimental replicates. Data are displayed as the mean ± SD. *P*-values were determined by Student's t-test and one-way ANOVA in panels. ***$P<0.001$, ****$P<0.0001$, ns: Not significant. CCK-8, Cell Counting Kit-8; ICC, intrahepatic cholangiocarcinoma; qRT-PCR, quantitative real-time polymerase chain reaction; H&E, hematoxylin and eosin; IHC, immunohistochemistry; SD, standard deviation; ANOVA, analysis of variance

the mRNA and protein levels (Supplementary Fig. 2A, B). The CCK-8 assay showed that NAT10 knockdown significantly inhibited the proliferation of ICC cells, whereas NAT10 overexpression increased it (Fig. 2C, Supplementary Fig. 2C). Live-cell imaging was used to photograph the cells every 2 h for 120 h, and the data were consistent with the CCK-8 (Fig. 2D, E, Supplementary Fig. 2D, E). A colony formation assay was performed to determine the long-term effects of NAT10 on ICC cell proliferation. After 8–12 days, NAT10 knockdown significantly reduced colony formation (Fig. 2F), whereas NAT10 overexpression significantly increased it (Supplementary Fig. 2F). To evaluate the effects of NAT10 on ICC in vivo, we constructed an animal xenograft model by injecting HuCCT1 cells subcutaneously into the left forelimbs of nude mice. Consistent with the in vitro results, the growth rate of NAT10-knockdown xenografts was slower than that of control xenografts (Fig. 2G-I). NAT10 also promotes ICC growth in vivo. In the in vivo experiment, we only presented the results from the shNAT10#1 group. In fact, we also validated the shNAT10#2 group. However, due to its significant inhibitory effect on ICC, no visible tumors in the nude mice of the shNAT10#2 group were observed by the end of the animal experiment. If the experiment had been extended, tumors might have developed in the shNAT10#2 group, but the tumor size in the control group would have exceeded the specified dimensions. Considering all factors, we ultimately decided to only present the results from the shNAT10#1 in vivo experiment. H&E staining of the subcutaneous tumor tissue of xenograft animal model showed angiogenesis in the control group, while necrosis of tumor cells appeared in the NAT10-knockdown group (Fig. 2J). Additionally, IHC and western blot confirmed down-regulated NAT10 expression in the NAT10-knockdown group (Fig. 2K, L). The data showed that NAT10 promotes ICC proliferation and may be an oncogene of ICC.

CCL2 is a downstream target of NAT10

To explore the role of NAT10 in the development of ICC and identify its downstream targets, we conducted ONT full-length transcriptome sequencing to examine changes after NAT10 knockdown. In RBE cells, 9 and 39 genes were consistently upregulated and downregulated by two independent shRNAs, respectively (Fig. 3A). We observed good agreement between the two independent shRNAs for the downregulated genes. GO analysis showed that differentially expressed genes were involved in apoptosis, cell surface receptor signaling pathways, immune response, secretion, and gene concentration in the extracellular regions and space, suggesting that NAT10 may have an important impact on ICC biology (Fig. 3B). CCL2 was concerned as the most prominent candidate target gene. qRT-PCR and western blot verified that NAT10 knockdown decreased the mRNA and protein levels of CCL2 (Fig. 3C, D). Additionally, CCL2 expression was significantly decreased in NAT10-knockdown tumors in vivo (Fig. 3E). The data indicate that NAT10 promotes CCL2 expression in ICC both in vitro and in vivo. Based on the acetyltransferase properties of NAT10, we further determined the regulatory mechanism of NAT10 on CCL2. RIP-quantitative polymerase chain reaction (RIP-qPCR) and coimmunoprecipitation (COIP) were conducted. The data showed that NAT10 exhibited strong binding and interaction with CCL2 mRNA, whereas the two proteins did not interact (Fig. 3F, G). In summary, CCL2 is a downstream target directly regulated by NAT10.

CCL2 promotes ICC growth in vitro and in vivo

To verify the tumor-promoting function of CCL2, we established stable CCL2-knockdown cell lines, which were validated by western blot (Fig. 4A). Using CCK-8 and live-cell imaging assays, we found that CCL2 knockdown significantly inhibited the proliferation of ICC cells (Fig. 4B-D). Additionally, CCL2 knockdown significantly inhibited colony formation (Fig. 4E). To confirm the role of CCL2 in ICC in vivo, we used a xenograft animal model where HuCCT1 cells were subcutaneously inoculated into the right forelimbs of nude mice. Consistent with the in vitro results, the growth rate of subcutaneous tumors in the CCL2-knockdown group was slower than that of tumors in the control group (Fig. 4F-H). Therefore, CCL2 promotes ICC growth in vivo. We stained the subcutaneous tumor tissues of xenograft animal models with H&E (Fig. 4I), and the knockdown of CCL2 was confirmed by IHC (Fig. 4J). The results showed that tumor

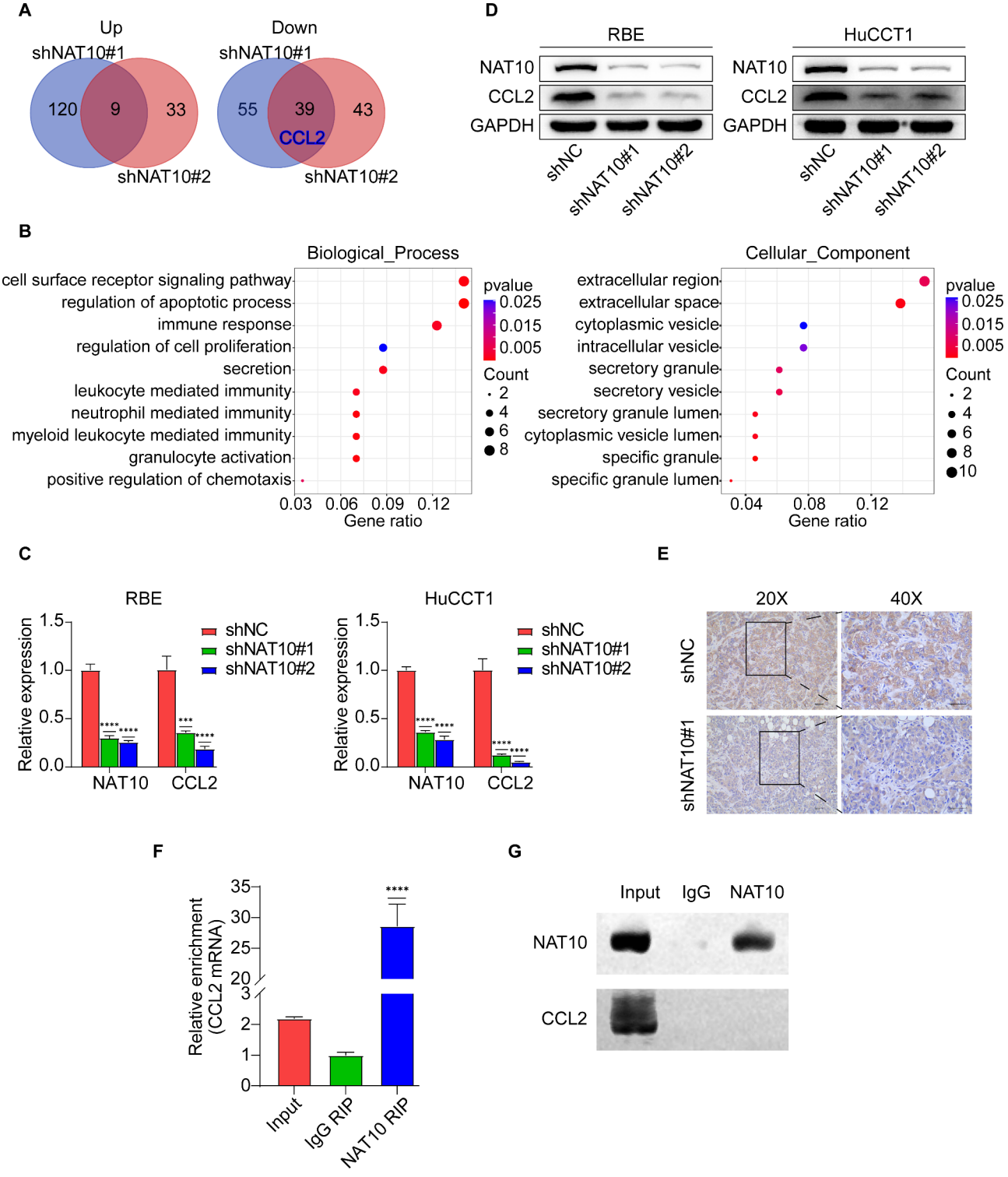

Fig. 3 CCL2 is a downstream target of NAT10. (A) RNA sequencing identified differentially expressed genes in NAT10-knockdown cells compared with control cells. (B) GO analysis of the NAT10-knockdown downregulated genes revealed the potential functions of NAT10 in regulating apoptosis, cell surface receptor signaling pathways, immune response, and secretion. (C and D) Knocking down NAT10 reduced CCL2 expression at the mRNA and protein levels in ICC cells. (E) IHC showing the expression of CCL2 in mouse tumor tissues. Scale bars: 40 μm. (F, G) NAT10 interacts with CCL2 mRNA but not protein. Data are representative of three or more independent experimental replicates. Data are displayed as the mean ± SD. *P*-values were determined by Student's t-test and one-way ANOVA in panels. ***$P < 0.001$, ****$P < 0.0001$. GO, Gene Ontology; ICC, intrahepatic cholangiocarcinoma; IHC, immunohistochemistry; SD, standard deviation; ANOVA, analysis of variance

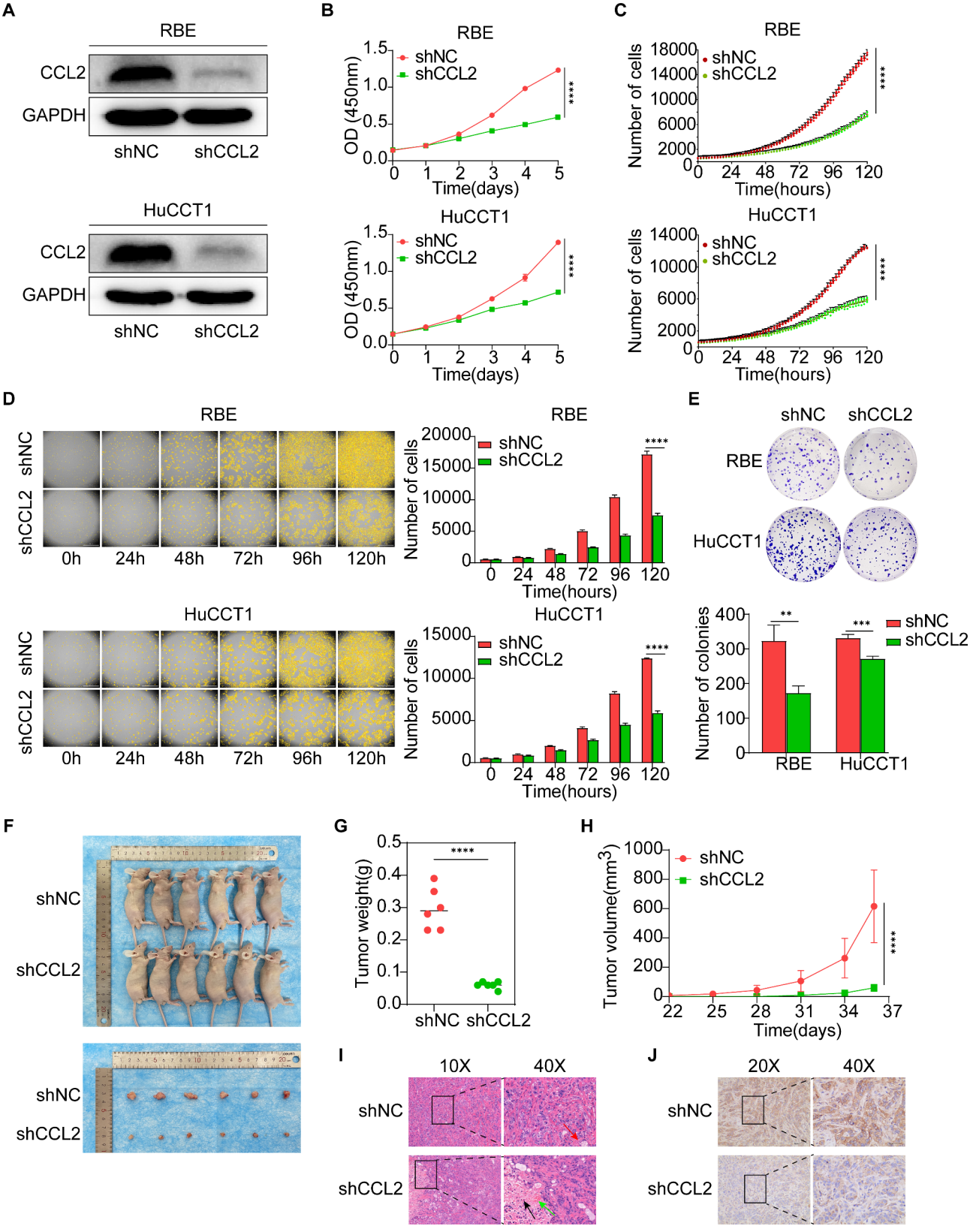

Fig. 4 (See legend on next page.)

(See figure on previous page.)

Fig. 4 Knocking down CCL2 inhibits ICC cell proliferation and tumor growth in mice. (A) CCL2-knockdown cell lines were constructed and verified at the protein level. (B) CCK-8 assays showed that knockdown of CCL2 significantly inhibited the proliferation of ICC cells. (C, D) Live-cell imaging showed that knockdown of CCL2 significantly inhibited the proliferation of ICC cells. Scale bars: 1000 μm. (E) Knockdown of CCL2 significantly reduced the colony-formation ability of ICC cells. (F-H) Knocking down CCL2 effectively inhibited the growth of ICC subcutaneous tumors in nude mice. Tumor size was measured every 3 days ($n=6$). (I) H&E staining of mouse tumor tissues after CCL2 knockdown. The red, black, and green arrows show angiogenesis, tumor cell necrosis, and hemorrhage, respectively. Scale bars: 100 (left panel) and 50 (right panel) μm. (J) IHC showing the expression of CCL2 in mouse tumor tissues. Scale bars: 40 μm. Data are representative of three or more independent experimental replicates. Data are displayed as the mean ± SD. *P*-values were determined by Student's t-test in panels. $^{**}P<0.01$, $^{***}P<0.001$, $^{****}P<0.0001$. CCK-8, Cell Counting Kit-8; ICC, intrahepatic cholangiocarcinoma; IHC, immunohistochemistry; H&E, hematoxylin and eosin; SD, standard deviation

angiogenesis occurred in the control group, while tumor cell necrosis and hemorrhage occurred in the tumor after CCL2 knockdown, which was consistent with the results of NAT10 knockdown.

Next, we infected NAT10-knockdown ICC cells with a lentivirus carrying CCL2 (Supplementary Fig. 3A) and performed CCK-8 assays and live-cell imaging, which showed that CCL2 overexpression partly rescued the loss of proliferation observed in NAT10-knockdown ICC cells (Supplementary Fig. 3B-D). Taken together, CCL2 is a downstream target of NAT10 and plays a role in promoting ICC growth both in vivo and in vitro.

NAT10 polarizes macrophages toward the M2 type through its regulation of CCL2

To study whether ICC cells can cause macrophage polarization and the type of polarization, we cultured RAW264.7 mouse macrophages with conditioned medium from ICC cells and performed qRT-PCR to detect the iNOS and Arg-1 levels after 24 h. Compared with control cells, co-cultured RAW264.7 was polarized (Fig. 5A). We also used a transwell chamber to co-culture ICC and RAW264.7 cells and obtained similar but more significant results (Fig. 5B). Additionally, we assessed this through flow cytometry. No difference in CD86 expression, representing M1 macrophages, was observed after co-culture; however, a significant increase in CD206 expression, representing M2 macrophages, was noted (Fig. 5C). These results indicate that ICC cells could polarize RAW264.7 cells toward the M2 type.

CCL2 can polarize macrophages toward the M2 type. Therefore, to assess whether the polarization of RAW264.7 cells to M2 type by ICC cells was dependent on NAT10, we first conducted immunofluorescence staining of the NAT10-knockdown tumors. The result showed that the expression of CD86, representing M1 macrophages in mice, was higher in the knockdown tumors than in the control tumors. In contrast, the expression of CD163, which represents M2 macrophages, was decreased (Fig. 5D). We subsequently knocked down NAT10 in ICC cells and used western blot and ELISA to detect the levels of CCL2 in the ICC cells and cell supernatants. NAT10 knockdown reduced the expression of CCL2 in both the cells and cell supernatants (Fig. 5E, F).

Lentivirus-mediated gene silencing was used to knock down CCL2 in RBE and HuCCT1 cells (Fig. 5G). Cells were co-cultured with RAW264.7 cells, and the levels of CD86 and CD206 were assessed using flow cytometry. Although ICC cells could still polarize RAW264.7 cells toward the M2 type after CCL2 knockdown, the effect was significantly reduced (Fig. 5H). We also performed immunofluorescence staining of the CCL2-knockdown tumors, and the results were consistent with those of the NAT10-knockdown tumors. The expression of CD86, representing M1 macrophages, was increased in CCL2-knockdown tumors, whereas that of CD163, representing M2 macrophages, was decreased (Fig. 5I). These results suggest that ICC cells can polarize macrophages toward the M2 type and that NAT10 plays an important role through its regulation of CCL2.

BBR can target the binding and inhibition of CCL2

Based on the anti-ICC function of NAT10 and CCL2, we attempted to screen their natural targeted inhibitors. Fortunately, a natural product, BBR was concerned, which presents high anti-inflammatory and anticancer activities. Molecular docking showed that the binding affinity of BBR with NAT10 and CCL2 was −8.3 and −6.3 kcal/mol, respectively (Fig. 6A). After treatment with BBR, HuCCT1 cells were analyzed using RNA sequencing. No significant change in NAT10 expression was fund after BBR treatment, although CCL2 was significantly decreased (Fig. 6B). The data suggested that BBR exerts antitumor effects on ICC by inhibiting CCL2. qRT-PCR and western blot also showed a significant down-regulation of CCL2 but not NAT10 at both the mRNA and protein levels (Fig. 6C, D). To further verify whether BBR could specifically bind to CCL2, we used SPR assay to detect its affinity. The data showed strong binding of BBR to CCL2, and the concentration gradient trend was significant. Specific binding occurred with an affinity of 423.4 μM (Fig. 6E, F).

Antitumor effects of BBR on ICC in vitro and in vivo

To demonstrate the effect of BBR on the proliferation of ICC cells, we treated RBE and HuCCT1 cells with different concentrations of BBR (0, 10, 20, 40, 80, 160, and 200 μM) and performed CCK-8 assays. BBR significantly reduced the viability of both cell lines. This inhibition

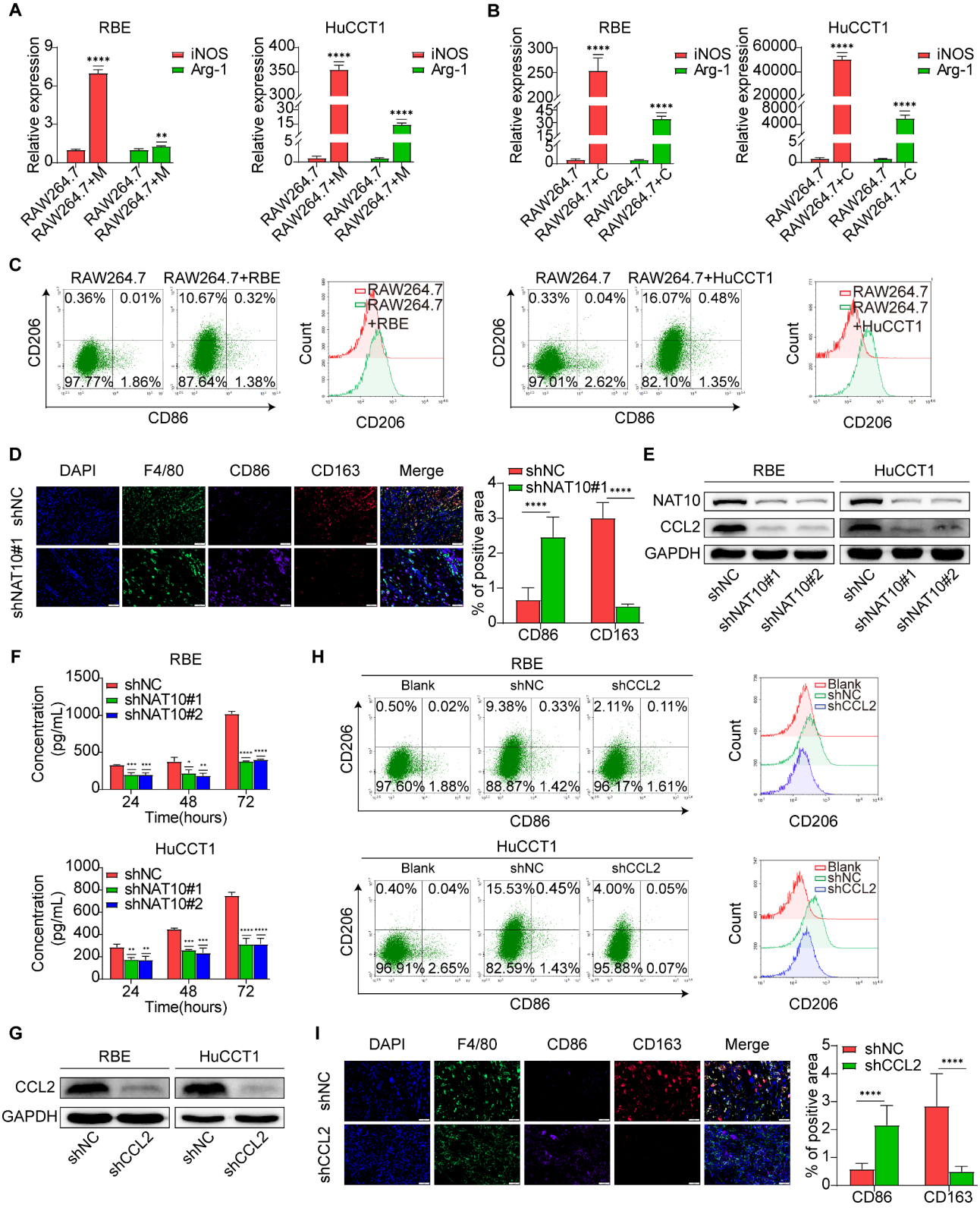

Fig. 5 (See legend on next page.)

(See figure on previous page.)

Fig. 5 NAT10 polarizes macrophages toward the M2 type through CCL2. (A) Macrophages were polarized by treating them with the supernatant of ICC cells for 24 h. (B) After co-culturing ICC cells and macrophages for 24 h, the macrophages underwent polarization. (C) Co-culturing ICC cells with macrophages for 24 h resulted in the polarization of macrophages towards the M2 phenotype. (D) Immunofluorescence showed that CD86 expression increased and CD163 expression decreased in NAT10-knockdown tumors ($n=6$). Scale bars: 50 μm. (E and F) Western blot and ELISA showed that NAT10 knockdown decreased CCL2 expression levels in ICC cells and cell supernatant. (G) CCL2-knockdown cell lines were constructed and verified at the protein level. (H) Flow cytometry confirmed that CCL2 knockdown reduced the polarization of macrophages toward M2. (I) Immunofluorescence showed that CD86 expression increased and CD163 expression decreased in CCL2-knockdown tumors ($n=6$). Scale bars: 50 μm. Data are representative of three or more independent experimental replicates. Data are displayed as the mean ± SD. *P*-values were determined by Student's t-test and one-way ANOVA in panels. *$P<0.05$, **$P<0.01$, ***$P<0.001$, ****$P<0.0001$. ICC, intrahepatic cholangiocarcinoma; ELISA, enzyme-linked immunosorbent assay; SD, standard deviation; ANOVA, analysis of variance

was time- and concentration-dependent (Fig. 7A). BBR had a stronger effect on HuCCT1 cells, showing a significant inhibitory effect at 48 h at a relatively low dose. We subsequently treated these two cell lines with BBR and conducted live-cell imaging. Significantly fewer cells were found in the BBR condition than in the DMSO condition, which was consistent with the results of the CCK-8 assay (Fig. 7B, C).

To deeply uncover the inhibitory effect of BBR on the proliferation of ICC cells, RBE and HuCCT1 cells were treated with BBR for 48 h, and changes in the cell cycle were detected using flow cytometry. After treatment with BBR, the percentage of the G0/G1 phase cells increased, whereas that of the S and G2/M phase cells significantly decreased (Supplementary Fig. 4A, B). We also used flow cytometry to assess apoptosis in RBE and HuCCT1 cells after 48 h of BBR treatment. BBR-induced apoptosis in both cell lines (Supplementary Fig. 4C, D). Taken together, the data suggest that BBR exerts antitumor effects by blocking ICC cells in the G0/G1 phase and inducing apoptosis.

To further verify the effect of BBR on tumor growth in vivo, HuCCT1 cells were subcutaneously transplanted into nude mice. When tumors appeared, the mice were randomly assigned into two groups, with six tumor-bearing mice per group, and BBR (50 mg/kg/day) or sterile water was administered orally. After 18 days of continuous administration of BBR, tumor size and weight were significantly lower than those in the control group (Fig. 7D-F). The tumor tissues were stained with H&E (Supplementary Fig. 4E), and IHC was used to detect the expressions of NAT10 and CCL2. No significant difference in the expression of NAT10 was found between the two groups; however, the expression of CCL2 in the tumors of the BBR group was significantly lower than that in the tumors of the control group (Supplementary Fig. 4F), which was consistent with the results of the in vitro experiments. Finally, immunofluorescence was used to detect macrophages in the tumors. Compared to the DMSO group, the expression of CD86, representing M1, was increased in the BBR group, whereas that of CD163, representing M2, was significantly decreased (Supplementary Fig. 4G), which was consistent with the results observed in NAT10- and CCL2-knockdown tumors. In summary, BBR inhibits the proliferation of ICC and affects the polarization of macrophages by specifically binding to CCL2, thereby playing an antitumor role.

Discussion

Post-transcriptional modification plays an important role in gene expression and function. Presently, more than 100 types of RNA modifications have been discovered, of which the most common is RNA methylation modification, namely m6A modification. The role of m6A in ICC has been reported to regulate the proliferation, metastasis, immunity, and TME of ICC [35–38]. Recently, another acetylation modification, known as ac4C modification, has begun to attract attention. As the only writer of ac4C, NAT10 is not only involved in several crucial cellular processes [39–41] but also the occurrence and development of tumors. Accumulating evidence shows that NAT10 plays an important role in the pathogenesis of multiple solid tumors [9–11, 42–44]. In this study, we observed a significant upregulation of NAT10 in CCA tissues. The high expression level of NAT10 was significantly correlated with the histological grade and primary tumor stage of patients with CCA. Additionally, we demonstrated that NAT10 promotes ICC cell proliferation and tumor growth in vivo. These findings suggest that NAT10 serves as a potential biomarker for predicting the onset and proliferation of ICC and could become a new therapeutic target.

The occurrence and development of tumors are not only related to tumor cells but are also affected by the TME. Macrophages are important components of the TME, infiltrated into the tumor by the recruitment of CCL2 in the TME and polarized into M2 macrophages by binding with CCL2 through CCR2 on the cell surface [25, 26]. M2 macrophages induced by CCL2 also secrete CCL2, which induces more macrophages to infiltrate into the tumor and polarize toward M2 [16, 17] and act on tumor cells to promote tumor progression [18, 26]. In addition to secreting CCL2, M2 macrophages also release cytokines, such as VEGF, PDGF, and TGF-β, to promote tumor cell EMT, angiogenesis, and ECM remodeling [18, 19]. Tumor cells and macrophages promote each other's progression through CCL2. In the present study, we confirm that CCL2 is the downstream target of NAT10

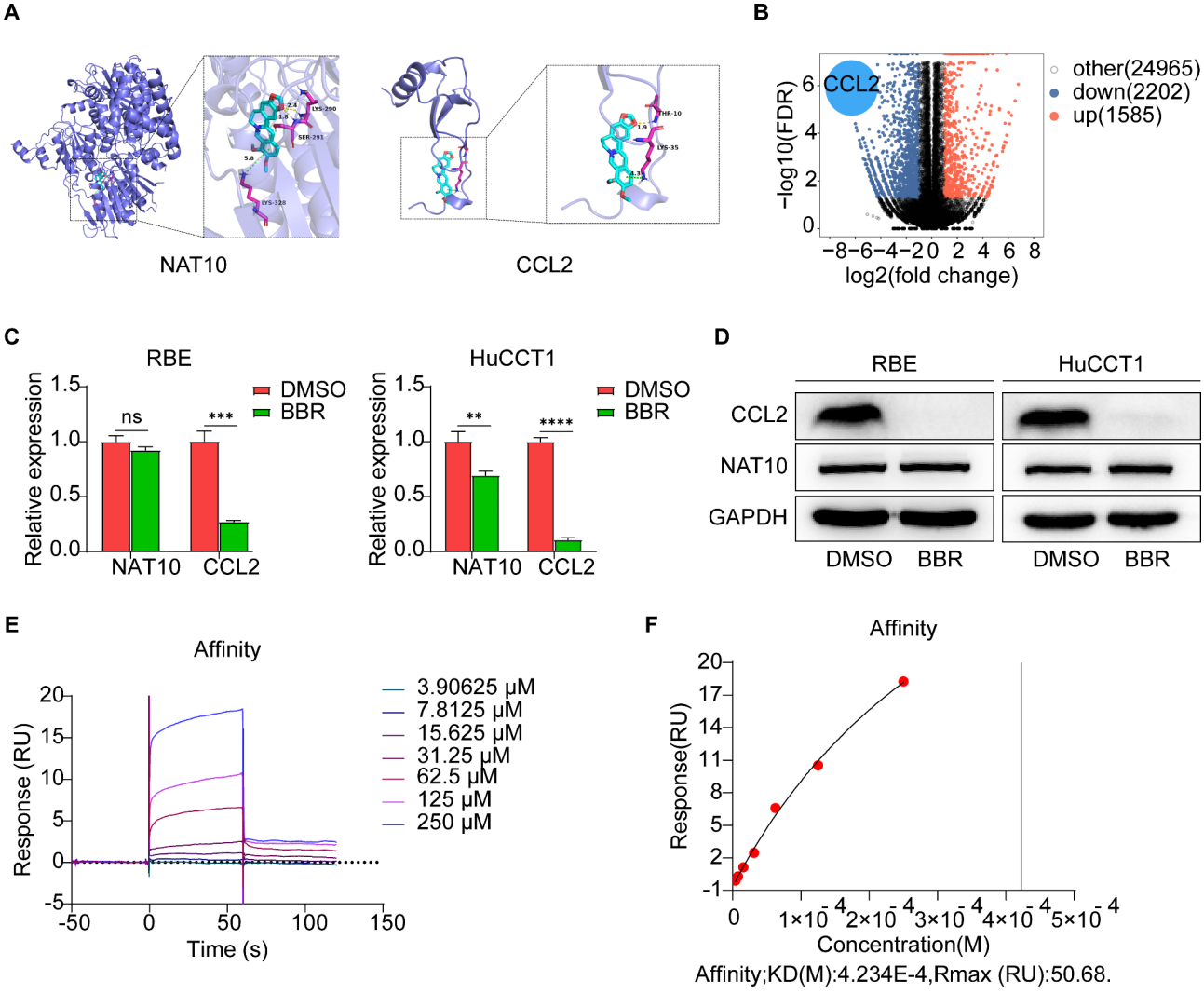

Fig. 6 BBR binds and inhibits CCL2. (A) Molecular docking simulation of BBR with NAT10 and CCL2. (B) Volcano plot of differentially expressed genes in HuCCT1 cells treated with BBR (20 μM, 48 h). (C and D) Expression of NAT10 and CCL2 at the mRNA and protein levels after BBR treatment. The doses used for RBE and HuCCT1 were 160 and 20 μM, respectively, and the treatment time for both was 48 h. (E and F) BBR bound specifically to CCL2 protein with a specific concentration gradient trend; its affinity was 423.4 μM. Data are representative of three or more independent experimental replicates. Data are displayed as the mean ± SD. *P*-values were determined by Student's t-test in panels. $^{**}P < 0.01$, $^{***}P < 0.001$, $^{****}P < 0.0001$, ns: Not significant. BBR, berberine; SD, standard deviation

in ICC. NAT10 promotes ICC cell proliferation and tumor growth in vivo through CCL2. The results of animal experiments showed that, although the tumor volume was smaller than that in the control group following the knockdown of NAT10 or CCL2, tumor cell necrosis and hemorrhage occurred. Presently, no report exists on whether NAT10 can affect the polarization of macrophages. We determined that CCL2 is the downstream target of NAT10, and CCL2 affects macrophage polarization. Further validation demonstrated that ICC can affect macrophage polarization through the regulation of CCL2 by NAT10. In both in vivo and in vitro experiments, NAT10 was found to polarize macrophages towards the M2 type by regulating CCL2. NAT10 is an acetylase, which can acetylate not only protein [45] but also mRNA [8]. Therefore, to further determine the potential regulatory mechanism of NAT10 on CCL2, we performed RIP-qPCR and COIP simultaneously. We found that NAT10 acts by binding to the mRNA of CCL2 in ICC rather than its protein. In the present study, we not only confirmed the intracellular regulatory mechanism by which NAT10 promotes ICC proliferation but also found the relationship between NAT10 and macrophage polarization. NAT10 in the nucleus of ICC cells binds to CCL2 mRNA, leading to an increase in CCL2 protein expression. The elevated CCL2 acts within ICC cells to promote ICC proliferation, while the CCL2 secreted into the extracellular environment can bind to receptors on the surface

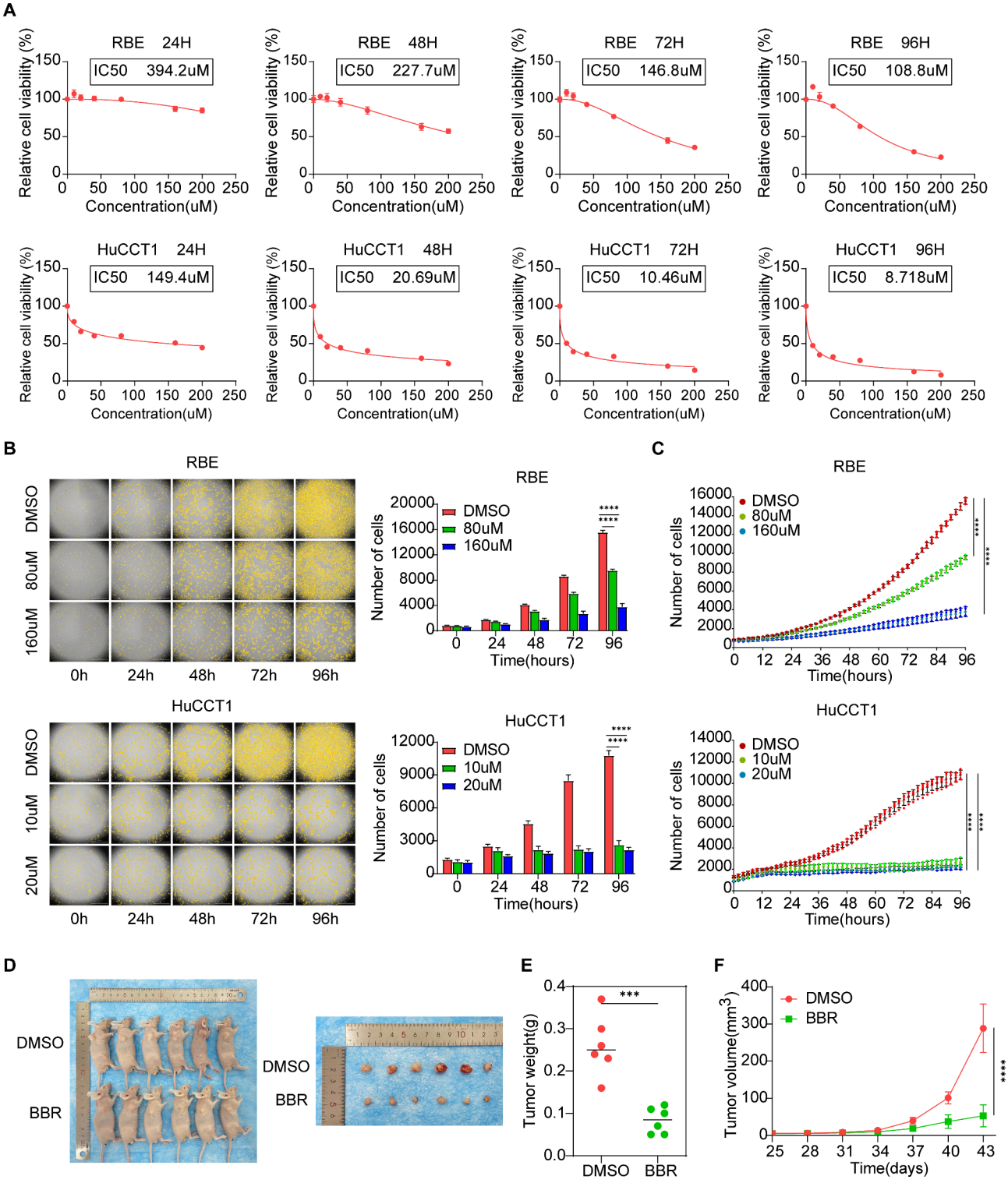

Fig. 7 BBR inhibits ICC cell proliferation and tumor growth in nude mice. HuCCT1 cells (1×10^7) were injected subcutaneously into the right forelimb of nude mice. When the tumor size reached approximately 5 mm^3, the mice were randomly assigned into two groups ($n = 6$). BBR was administered orally at a dose of 50 mg/kg/day, while the control group received sterile water containing DMSO for 18 days. (A) The IC50 values of BBR in ICC cells at different time points (24, 48, 72, and 96 h). (B and C) BBR significantly inhibited the proliferation of ICC cells. Scale bars: 1000 μm. (D-F) BBR effectively inhibited the growth of ICC subcutaneous tumors in nude mice. Tumor size was measured every 3 days ($n = 6$). Data are representative of three or more independent experimental replicates. Data are displayed as the mean ± SD. *P*-values were determined by Student's t-test and one-way ANOVA in panels. ***$P < 0.001$, ****$P < 0.0001$. BBR, berberine; ICC, intrahepatic cholangiocarcinoma; DMSO, dimethyl sulfoxide; SD, standard deviation; ANOVA, analysis of variance

of macrophages, inducing their polarization toward the M2 type (Fig. 8). NAT10 and CCL2 are likely to serve as potential diagnostic markers and therapeutic targets for ICC because they play an important role in ICC.

ICC has no specific targeted drugs. BBR is a small isoquinoline alkaloid that can be extracted from *Rhizoma coptidis* and *Hydrastis canadensis* [46, 47]. It has been found to have therapeutic effects on many diseases [48–51]. Accumulating studies have reported that BBR also has antitumor effects [52–57]. Our study demonstrates that as the downstream target of NAT10, CCL2, a chemokine, plays an important role in both tumor and inflammation. CCL2 also plays a critical role in ICC cell proliferation and macrophage polarization. Our results suggest that BBR can specifically bind to CCL2 and thereby play an antitumor role on ICC. BBR primarily exerts its effects by inhibiting tumor cell proliferation and promoting apoptosis. For different tumor cells, BBR can block them at different stages of the cell cycle [58–62]. This study confirmed that BBR can arrest ICC cells in the G0/G1 phase and promote cell apoptosis. Additionally, immunofluorescence staining was performed on the subcutaneous tumor tissues of nude mice in the BBR-treated group. The expression of CD86, representing M1 macrophages, was significantly upregulated, while that of CD163, representing M2 macrophages, was significantly downregulated. These findings were consistent with the results of CCL2 knockdown. Our results also indicate that BBR can not only play an antitumor role on ICC cells through CCL2 but also regulate macrophage polarization and affect the TME by influencing the level of CCL2 secreted into the extracellular cell. Presently, the research methods for targeted drugs are mainly large-scale screening through activity-based protein profiling (ABPP) and molecular docking [63, 64]. However, these methods are mainly based on molecular structure. In our study,

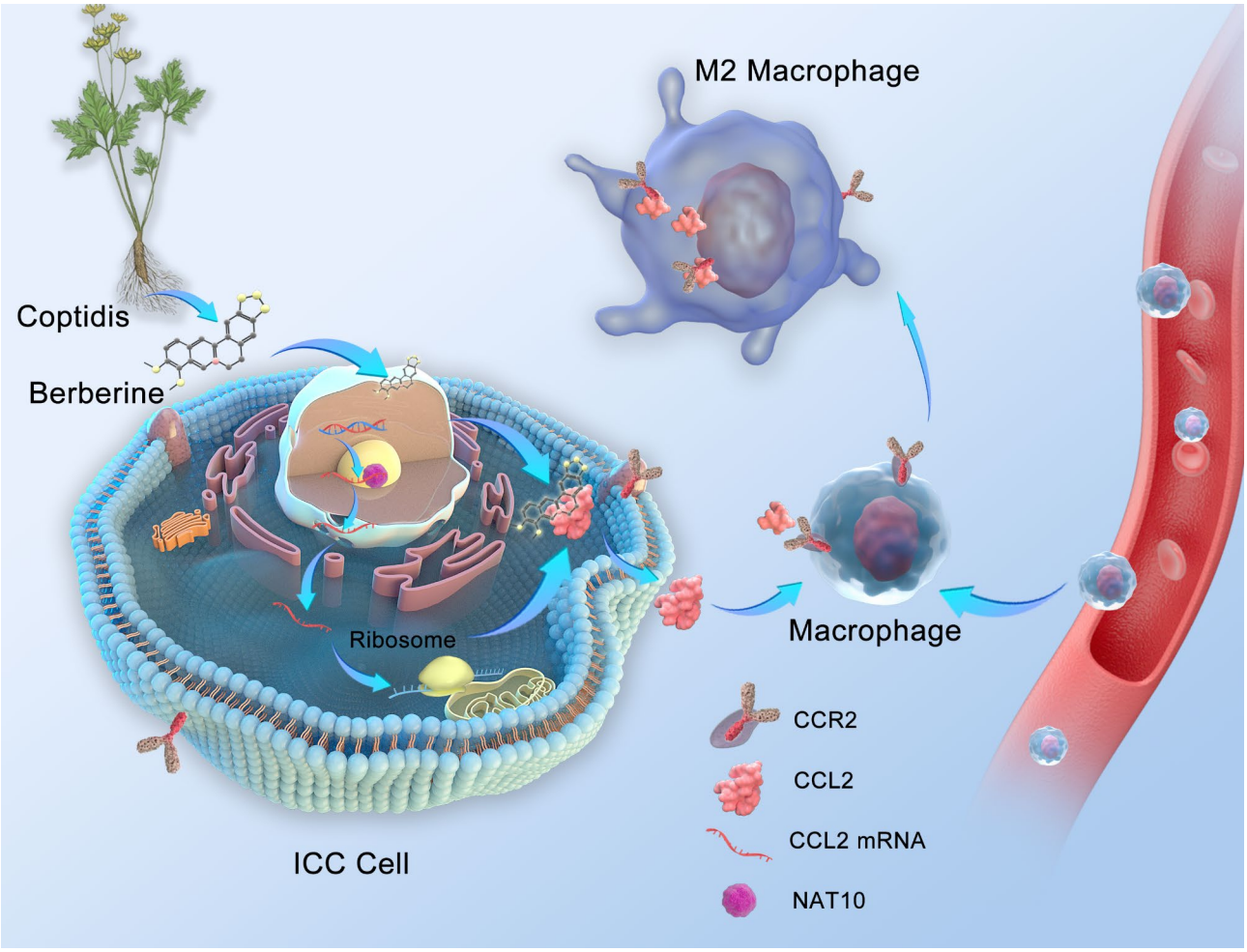

Fig. 8 Mechanism of action of NAT10 and BBR in ICC and macrophage polarization. NAT10 in the nucleus of ICC cells binds to CCL2 mRNA, leading to an increase in CCL2 protein expression. The elevated CCL2 acts within ICC cells to promote ICC proliferation, while the CCL2 secreted into the extracellular environment can bind to receptors on the surface of macrophages, inducing their polarization toward the M2 type. In contrast, BBR can target the CCL2 protein within ICC cells and inhibit ICC proliferation. BBR, berberine; ICC, intrahepatic cholangiocarcinoma

we adopted a different approach, namely the functional consistency of the drug and the molecule. This discovery not only provides a potential targeted therapeutic drug for the treatment of ICC but also offers a possible new method for the study of targeted drugs.

In summary, we found that NAT10 expression is upregulated in ICC and is associated with poor clinicopathological features in patients with tumors. Mechanically, NAT10 promotes ICC proliferation through the regulation of CCL2 mRNA and causes macrophages to become M2-type. BBR inhibited the proliferation of ICC and macrophage M2-type polarization by targeting CCL2. These findings not only provide new potential diagnostic markers and therapeutic targets for ICC but also offer possible targeted therapeutic strategies.

Abbreviations

ICC	intrahepatic cholangiocarcinoma
NAT10	N-acetyltransferase 10
TMA	tissue microarray
CCA	cholangiocarcinoma
CCL2	C-C motif chemokine ligand 2
SPR	surface plasmon resonance
BBR	berberine
TME	tumor microenvironment
TMAs	tumor-associated macrophages
CCR2	C-C motif chemokine receptor 2
MCP-1	monocyte chemoattractant protein-1
STR	short tandem repeats
IHC	immunohistochemistry
H&E	hematoxylin and eosin
ONT	Oxford Nanopore Technologies
COIP	coimmunoprecipitation
ELISA	enzyme-linked immunosorbent assay
TCGA	The Cancer Genome Atlas
STAD	stomach adenocarcinoma
COAD	colon adenocarcinoma
READ	rectum adenocarcinoma
OS	overall survival
DFS	disease-free survival
VEGF	vascular endothelial growth factor
PDGF	platelet-derived growth factor
TGF-β	transforming growth factor-β
EMT	epithelial-mesenchymal transition
ECM	extracellular matrix
ac4C	N4-acetylcytidine
CCK-8	Cell Counting Kit-8
ACC	adrenocortical carcinoma
HNSC	head and neck squamous cell carcinoma
KICH	kidney chromophobe
KIRP	kidney renal papillary cell carcinoma
LIHC	liver hepatocellular carcinoma
UVM	uveal melanoma
shRNA	short hairpin RNA
GO	Gene Ontology
KEGG	Kyoto Encyclopedia of Genes and Genomes
qRT-PCR	quantitative real-time polymerase chain reaction
DMSO	dimethyl sulfoxide
SD	standard deviation
ANOVA	analysis of variance
ABPP	activity-based protein profiling

Supplementary Information

The online version contains supplementary material available at https://doi.org/10.1186/s12967-024-05664-z.

Supplementary Material 1

Supplementary Material 2

Supplementary Material 3

Supplementary Material 4

Supplementary Material 5

Acknowledgements
All mice experiments were approved by the Ethics Committee of the First Hospital of Lanzhou University (approval number: LDYYLL-2024-38).

Author contributions
TC, JL, and WM designed the experiment. TC completed the experiment, data analysis, and the writing of the manuscript draft. ZB, JD, and YL analyzed and interpreted the data and reviewed the manuscript. JD and YL participated in the bioinformatics analysis. ZB, JL, and WM supervised the study, provided funding and resources, and revised the manuscript. All authors reviewed and approved the final manuscript.

Funding
This study was supported by the National Natural Science Foundation of China (grant numbers: 82060551; 82060666).

Data availability
The data that support the findings of this study are available from the corresponding authors upon reasonable request.

Declarations

Ethics approval and consent to participate
Not applicable.

Consent for publication
Not applicable.

Competing interests
The authors declare no competing interests.

Author details
[1]The First Clinical Medical College, Lanzhou University, Lanzhou 730000, China
[2]Department of Hepatobiliary Surgery, Affiliated Hospital of North Sichuan Medical College, Nanchong 637600, China
[3]School of Pharmacy, Lanzhou University, Lanzhou 730000, China
[4]The Department of General Surgery, The First Hospital of Lanzhou University, Lanzhou 730000, China
[5]Gansu Province Key Laboratory Biotherapy and Regenerative Medicine, Lanzhou 730000, China

Received: 19 June 2024 / Accepted: 12 September 2024
Published online: 30 September 2024

References

1. Rizvi S, Gores GJ. Pathogenesis, diagnosis, and management of Cholangiocarcinoma. Gastroenterology. 2013;145:1215–29.
2. Rizvi S, Khan SA, Hallemeier CL, Kelley RK, Gores GJ. Cholangiocarcinoma — evolving concepts and therapeutic strategies. Nat Reviews Clin Oncol. 2017;15:95–111.
3. Khan SA, Taylor-Robinson SD, Toledano MB, Beck A, Elliott P, Thomas HC. Changing international trends in mortality rates for liver, biliary and pancreatic tumours. J Hepatol. 2002;37:806–13.
4. Patel T. Worldwide trends in mortality from biliary tract malignancies. BMC Cancer. 2002;2:10.
5. Bridgewater J, Galle PR, Khan SA, Llovet JM, Park JW, Patel T, Pawlik TM, Gores GJ. Guidelines for the diagnosis and management of intrahepatic cholangiocarcinoma. J Hepatol. 2014;60:1268–89.

6. Spolverato G, Vitale A, Cucchetti A, Popescu I, Marques HP, Aldrighetti L, Gamblin TC, Maithel SK, Sandroussi C, Bauer TW, et al. Can hepatic resection provide a long-term cure for patients with intrahepatic cholangiocarcinoma? Cancer. 2015;121:3998–4006.
7. Franssen S, Holster JJ, Jolissaint JS, Nooijen LE, Cercek A, D'Angelica MI, Homs MYV, Wei AC, Balachandran VP, Drebin JA, et al. Gemcitabine with Cisplatin Versus hepatic arterial infusion Pump Chemotherapy for Liver-Confined Unresectable Intrahepatic Cholangiocarcinoma. Ann Surg Oncol. 2024;31:115–24.
8. Arango D, Sturgill D, Alhusaini N, Dillman AA, Sweet TJ, Hanson G, Hosogane M, Sinclair WR, Nanan KK, Mandler MD, et al. Acetylation of Cytidine in mRNA promotes translation efficiency. Cell. 2018;175:1872–e18861824.
9. Li Z, Li D, Yang T, Yao C. NAT10 promotes the tumorigenesis and progression of laryngeal squamous cell carcinoma through ac4C modification of FOXM1 mRNA. Cancer Biol Ther. 2023;24:2274143.
10. Pan Z, Bao Y, Hu M, Zhu Y, Tan C, Fan L, Yu H, Wang A, Cui J, Sun G. Role of NAT10-mediated ac4C-modified HSP90AA1 RNA acetylation in ER stress-mediated metastasis and lenvatinib resistance in hepatocellular carcinoma. Cell Death Discovery. 2023;9:56.
11. Chen X, Hao Y, Liu Y, Zhong S, You Y, Ao K, Chong T, Luo X, Yin M, Ye M, et al. NAT10/ac4C/FOXP1 promotes malignant progression and facilitates immunosuppression by reprogramming glycolytic metabolism in Cervical Cancer. Adv Sci. 2023;10:e2302705.
12. Zhang Y, Jing Y, Wang Y, Tang J, Zhu X, Jin WL, Wang Y, Yuan W, Li X, Li X. NAT10 promotes gastric cancer metastasis via N4-acetylated COL5A1. Signal Transduct Target Ther. 2021;6:173.
13. Funes SC, Rios M, Escobar-Vera J, Kalergis AM. Implications of macrophage polarization in autoimmunity. Immunology. 2018;154:186–95.
14. Arneth B. Tumor Microenvironment. *Medicina (Kaunas)* 2019, 56.
15. Petty AJ, Yang Y. Tumor-associated macrophages: implications in cancer immunotherapy. Immunotherapy. 2017;9:289–302.
16. Sierra-Filardi E, Nieto C, Domínguez-Soto A, Barroso R, Sánchez-Mateos P, Puig-Kroger A, López-Bravo M, Joven J, Ardavín C, Rodríguez-Fernández JL, et al. CCL2 shapes macrophage polarization by GM-CSF and M-CSF: identification of CCL2/CCR2-dependent gene expression profile. J Immunol. 2014;192:3858–67.
17. Chen Y, Song Y, Du W, Gong L, Chang H, Zou Z. Tumor-associated macrophages: an accomplice in solid tumor progression. J Biomed Sci. 2019;26:78.
18. Izumi K, Fang LY, Mizokami A, Namiki M, Li L, Lin WJ, Chang C. Targeting the androgen receptor with siRNA promotes prostate cancer metastasis through enhanced macrophage recruitment via CCL2/CCR2-induced STAT3 activation. EMBO Mol Med. 2013;5:1383–401.
19. Chanmee T, Ontong P, Konno K, Itano N. Tumor-associated macrophages as major players in the tumor microenvironment. Cancers (Basel). 2014;6:1670–90.
20. Xu LL, Warren MK, Rose WL, Gong W, Wang JM. Human recombinant monocyte chemotactic protein and other C-C chemokines bind and induce directional migration of dendritic cells in vitro. J Leukoc Biol. 1996;60:365–71.
21. Carr MW, Roth SJ, Luther E, Rose SS, Springer TA. Monocyte chemoattractant protein 1 acts as a T-lymphocyte chemoattractant. Proc Natl Acad Sci U S A. 1994;91:3652–6.
22. Lim SY, Yuzhalin AE, Gordon-Weeks AN, Muschel RJ. Targeting the CCL2-CCR2 signaling axis in cancer metastasis. Oncotarget. 2016;7:28697–710.
23. Kulbe H, Levinson NR, Balkwill F, Wilson JL. The chemokine network in cancer–much more than directing cell movement. Int J Dev Biol. 2004;48:489–96.
24. Yoshimura T. The chemokine MCP-1 (CCL2) in the host interaction with cancer: a foe or ally? Cell Mol Immunol. 2018;15:335–45.
25. Yang H, Zhang Q, Xu M, Wang L, Chen X, Feng Y, Li Y, Zhang X, Cui W, Jia X. CCL2-CCR2 axis recruits tumor associated macrophages to induce immune evasion through PD-1 signaling in esophageal carcinogenesis. Mol Cancer. 2020;19:41.
26. Li D, Ji H, Niu X, Yin L, Wang Y, Gu Y, Wang J, Zhou X, Zhang H, Zhang Q. Tumor-associated macrophages secrete CC-chemokine ligand 2 and induce tamoxifen resistance by activating PI3K/Akt/mTOR in breast cancer. Cancer Sci. 2019;111:47–58.
27. Tu W, Gong J, Zhou Z, Tian D, Wang Z. TCF4 enhances hepatic metastasis of colorectal cancer by regulating tumor-associated macrophage via CCL2/CCR2 signaling. Cell Death Dis. 2021;12:882.
28. Young MD, Wakefield MJ, Smyth GK, Oshlack A. Gene ontology analysis for RNA-seq: accounting for selection bias. Genome Biol. 2010;11:R14.
29. Mao X, Cai T, Olyarchuk JG, Wei L. Automated genome annotation and pathway identification using the KEGG Orthology (KO) as a controlled vocabulary. Bioinformatics. 2005;21:3787–93.
30. O'Boyle NM, Banck M, James CA, Morley C, Vandermeersch T, Hutchison GR. Open Babel: an open chemical toolbox. J Cheminform. 2011;3:33.
31. Eberhardt J, Santos-Martins D, Tillack AF, Forli S. AutoDock Vina 1.2.0: new docking methods, expanded force field, and Python Bindings. J Chem Inf Model. 2021;61:3891–8.
32. Del Conte A, Monzon AM, Clementel D, Camagni GF, Minervini G, Tosatto SCE, Piovesan D. RING-PyMOL: residue interaction networks of structural ensembles and molecular dynamics. Bioinformatics 2023, 39.
33. Love MI, Huber W, Anders S. Moderated estimation of Fold change and dispersion for RNA-seq data with DESeq2. Genome Biol. 2014;15:550.
34. Tang Z, Kang B, Li C, Chen T, Zhang Z. GEPIA2: an enhanced web server for large-scale expression profiling and interactive analysis. Nucleic Acids Res. 2019;47:W556–60.
35. Gao Y, Yu M, Liu Z, Liu Y, Kong Z, Zhu C, Qin X, Li Y, Tang L. m6A demethylase ALKBH5 maintains stemness of intrahepatic cholangiocarcinoma by sustaining BUB1B expression and cell proliferation. Translational Oncol. 2024;41:101858.
36. Xiang D, Gu M, Liu J, Dong W, Yang Z, Wang K, Fu J, Wang H. m6A RNA methylation-mediated upregulation of HLF promotes intrahepatic cholangiocarcinoma progression by regulating the FZD4/β-catenin signaling pathway. Cancer Lett. 2023;560:216144.
37. Zhou S, Yang K, Chen S, Lian G, Huang Y, Yao H, Zhao Y, Huang K, Yin D, Lin H, Li Y. CCL3 secreted by hepatocytes promotes the metastasis of intrahepatic cholangiocarcinoma by VIRMA-mediated N6-methyladenosine (m(6)A) modification. J Transl Med. 2023;21:43.
38. Qiu X, Yang S, Wang S, Wu J, Zheng B, Wang K, Shen S, Jeong S, Li Z, Zhu Y, et al. M(6)a demethylase ALKBH5 regulates PD-L1 expression and Tumor Immunoenvironment in Intrahepatic Cholangiocarcinoma. Cancer Res. 2021;81:4778–93.
39. Chi YH, Haller K, Peloponese JM Jr., Jeang KT. Histone acetyltransferase hALP and nuclear membrane protein hsSUN1 function in de-condensation of mitotic chromosomes. J Biol Chem. 2007;282:27447–58.
40. Fu D, Collins K. Purification of human telomerase complexes identifies factors involved in telomerase biogenesis and telomere length regulation. Mol Cell. 2007;28:773–85.
41. Ito S, Horikawa S, Suzuki T, Kawauchi H, Tanaka Y, Suzuki T, Suzuki T. Human NAT10 is an ATP-dependent RNA acetyltransferase responsible for N4-acetylcytidine formation in 18 S ribosomal RNA (rRNA). J Biol Chem. 2014;289:35724–30.
42. Jin C, Wang T, Zhang D, Yang P, Zhang C, Peng W, Jin K, Wang L, Zhou J, Peng C, et al. Acetyltransferase NAT10 regulates the Wnt/β-catenin signaling pathway to promote colorectal cancer progression via ac4C acetylation of KIF23 mRNA. J Experimental Clin Cancer Res. 2022;41:345.
43. Feng Z, Li K, Qin K, Liang J, Shi M, Ma Y, Zhao S, Liang H, Han D, Shen B, et al. The LINC00623/NAT10 signaling axis promotes pancreatic cancer progression by remodeling ac4C modification of mRNA. J Hematol Oncol. 2022;15:112.
44. Wang G, Zhang M, Zhang Y, Xie Y, Zou J, Zhong J, Zheng Z, Zhou X, Zheng Y, Chen B, Liu C. NAT10-mediated mRNA N4-acetylcytidine modification promotes bladder cancer progression. Clin Translational Med. 2022;12:e738.
45. Liu HY, Liu YY, Yang F, Zhang L, Zhang FL, Hu X, Shao ZM, Li DQ. Acetylation of MORC2 by NAT10 regulates cell-cycle checkpoint control and resistance to DNA-damaging chemotherapy and radiotherapy in breast cancer. Nucleic Acids Res. 2020;48:3638–56.
46. Chen XW, Di YM, Zhang J, Zhou ZW, Li CG, Zhou SF. Interaction of herbal compounds with biological targets: a case study with berberine. *ScientificWorldJournal* 2012, 2012:708292.
47. Tillhon M, Guamán Ortiz LM, Lombardi P, Scovassi AI. Berberine: new perspectives for old remedies. Biochem Pharmacol. 2012;84:1260–7.
48. Zhang M, Wang CM, Li J, Meng ZJ, Wei SN, Li J, Bucala R, Li YL, Chen L. Berberine protects against palmitate-induced endothelial dysfunction: involvements of upregulation of AMPK and eNOS and downregulation of NOX4. Mediators Inflamm. 2013;2013:260464.
49. Ma X, Yu X, Li R, Cui J, Yu H, Ren L, Jiang J, Zhang W, Wang L. Berberine-silybin salt achieves improved anti-nonalcoholic fatty liver disease effect through regulating lipid metabolism. J Ethnopharmacol. 2024;319:117238.
50. Heidarian E, Rafieian-Kopaei M, Khoshdel A, Bakhshesh M. Metabolic effects of berberine on liver phosphatidate phosphohydrolase in rats fed on high lipogenic diet: an additional mechanism for the hypolipidemic effects of berberine. Asian Pac J Trop Biomed. 2014;4:S429–435.

51. Ansari N, Khodagholi F. Natural products as promising drug candidates for the treatment of Alzheimer's disease: molecular mechanism aspect. Curr Neuropharmacol. 2013;11:414–29.
52. Chu SC, Yu CC, Hsu LS, Chen KS, Su MY, Chen PN. Berberine reverses epithelial-to-mesenchymal transition and inhibits metastasis and tumor-induced angiogenesis in human cervical cancer cells. Mol Pharmacol. 2014;86:609–23.
53. Choi MS, Oh JH, Kim SM, Jung HY, Yoo HS, Lee YM, Moon DC, Han SB, Hong JT. Berberine inhibits p53-dependent cell growth through induction of apoptosis of prostate cancer cells. Int J Oncol. 2009;34:1221–30.
54. Hwang JM, Kuo HC, Tseng TH, Liu JY, Chu CY. Berberine induces apoptosis through a mitochondria/caspases pathway in human hepatoma cells. Arch Toxicol. 2006;80:62–73.
55. Piyanuch R, Sukhthankar M, Wandee G, Baek SJ. Berberine, a natural isoquinoline alkaloid, induces NAG-1 and ATF3 expression in human colorectal cancer cells. Cancer Lett. 2007;258:230–40.
56. Liu Y, Hua W, Li Y, Xian X, Zhao Z, Liu C, Zou J, Li J, Fang X, Zhu Y. Berberine suppresses colon cancer cell proliferation by inhibiting the SCAP/SREBP-1 signaling pathway-mediated lipogenesis. Biochem Pharmacol. 2020;174:113776.
57. Li G, Zhang C, Liang W, Zhang Y, Shen Y, Tian X. Berberine regulates the Notch1/PTEN/PI3K/AKT/mTOR pathway and acts synergistically with 17-AAG and SAHA in SW480 colon cancer cells. Pharm Biol. 2021;59:21–30.
58. Xiao Y, Tian C, Huang T, Han B, Wang M, Ma H, Li Z, Ye X, Li X. 8-Cetylberberine inhibits growth of lung cancer in vitro and in vivo. Life Sci. 2018;192:259–69.
59. Su YH, Tang WC, Cheng YW, Sia P, Huang CC, Lee YC, Jiang HY, Wu MH, Lai IL, Lee JW, Lee KH. Targeting of multiple oncogenic signaling pathways by Hsp90 inhibitor alone or in combination with berberine for treatment of colorectal cancer. Biochim Biophys Acta. 2015;1853:2261–72.
60. Eo SH, Kim JH, Kim SJ. Induction of G_2/M arrest by Berberine via activation of PI3K/Akt and p38 in human Chondrosarcoma Cell line. Oncol Res. 2014;22:147–57.
61. Gao X, Wang J, Li M, Wang J, Lv J, Zhang L, Sun C, Ji J, Yang W, Zhao Z, Mao W. Berberine attenuates XRCC1-mediated base excision repair and sensitizes breast cancer cells to the chemotherapeutic drugs. J Cell Mol Med. 2019;23:6797–804.
62. Wu HL, Chuang TY, Al-Hendy A, Diamond MP, Azziz R, Chen YH. Berberine inhibits the proliferation of human uterine leiomyoma cells. Fertil Steril. 2015;103:1098–106.
63. Feng P, Chen D, Wang X, Li Y, Li Z, Li B, Zhang Y, Li W, Zhang J, Ye J, et al. Inhibition of the m(6)a reader IGF2BP2 as a strategy against T-cell acute lymphoblastic leukemia. Leukemia. 2022;36:2180–8.
64. Luo P, Zhang Q, Zhong TY, Chen JY, Zhang JZ, Tian Y, Zheng LH, Yang F, Dai LY, Zou C, et al. Celastrol mitigates inflammation in sepsis by inhibiting the PKM2-dependent Warburg effect. Mil Med Res. 2022;9:22.

Publisher's note